*Geophys. J. Int.* (1999) **136,** 171–179

# A seismic profile of the upper mantle along the southwestern edge of the Philippine Sea plate using short-period array data

Robert L. Nowack,[1] Erkan Ay,[1] Wang-Ping Chen[2] and Bor-Shouh Huang[3]

[1] *Department of Earth & Atmospheric Sciences, Purdue University, West Lafayette,* IN 47907, *USA*

[2] *Department of Geology, University of Illinois, Urbana,* IL 61801, *USA*

[3] *Institute of Earth Sciences, Academia Sinica, Taipei, Taiwan*

Accepted 1998 August 11. Received 1998 August 5; in original form 1997 October 28

## SUMMARY

We investigated the structure of the *P*-wave velocity (*Vp*) in the upper mantle beneath the southwestern edge of the Philippine Sea plate using traveltimes and waveforms from a dense, short-period seismic array of approximately 75 seismographs in Taiwan. Using the seismograms from 39 shallow-focus earthquakes, a composite seismic profile was constructed for a distance range of up to 4000 km. We picked the traveltimes of the first arrivals to construct a smoothly varying model for *Vp* which also served as a basis for static corrections. After band-pass filtering and deconvolution to remove effects of source-time functions and attenuation, we modelled the waveforms and triplicated arrivals in order to constrain the nature of the upper-mantle discontinuities. Finally, after slant stacking, the entire observed wavefield was downward continued to obtain a regional model TS.406. This model includes a small low-velocity zone between depths of 105 and 190 km, and then a gradual increase in *Vp* down to the depth of 406 km. At this discontinuity, *Vp* increases by 5.5 per cent. The *P*-wave velocity then varies linearly in the transition zone with a moderate gradient of 0.0027 km $s^{-1}$ $km^{-1}$ until the base of the transition zone at 662 km, where *Vp* increases by 5.4 per cent. When compared with other models for the Philippine Sea region and average global models, model TS.406 has lower velocities above a depth of 300 km and then faster *Vp* in the upper part of the transition zone. For example, above 300 km the TS.406 model is slower than IASP91 by 1.5 per cent, but in the upper transition zone (406 to 571 km), it is faster by 1.2 per cent. Thus, the moderate-amplitude anomaly of fast *Vp* in the middle of the transition zone reported by tomographic studies seems to occur at shallower depths. Furthermore, unlike the pronounced Northern Philippine Sea anomaly, *Vp* near the bottom of the transition zone is close to the global average under the southwestern edge of the Philippine Sea.

**Key words:** body waves, transition zone, upper mantle.

## INTRODUCTION

The tectonic setting of the Philippine Sea plate is unique in that the plate is mostly surrounded by convergent zones. The Philippine Sea is a back-arc basin related to westward subduction of the Pacific plate along the Izu-Bonin and Mariana arcs. This back-arc basin, in turn, subducts westward beneath Eurasia and the South China Sea (Fig. 1) (e.g. Seno, Stein & Gripp 1993).

The structure of the upper mantle beneath the Philippine Sea plate is also complex. Images from tomographic analysis of *P*-wave traveltimes show a pronounced anomaly of fast *P*-wave velocities (*Vp*) in the middle of the transition zone of the mantle under much of the northern Philippine Sea and adjacent regions (Fukao *et al.* 1992; van der Hilst *et al.* 1991, 1993). These subhorizontal anomalies in *Vp* have been interpreted as remnants of subducted slab of the Pacific plate and therefore are closely related to the plate-tectonic history of the region (van der Hilst & Seno 1993).

Using short-period and broad-band data from seismic arrays in Taiwan and Japan, Brudzinski *et al.* (1997) studied the northern Philippine Sea anomaly in detail. In contrast to the results of tomography, they found that this anomaly occurs just above the top of the lower mantle, over a limited region along the northwestern corner of the Philippine Sea plate.

The observation that the northern Philippine Sea anomaly does not extend beyond the northwestern edge of the Philippine Sea plate is supported by two other independent studies. Using

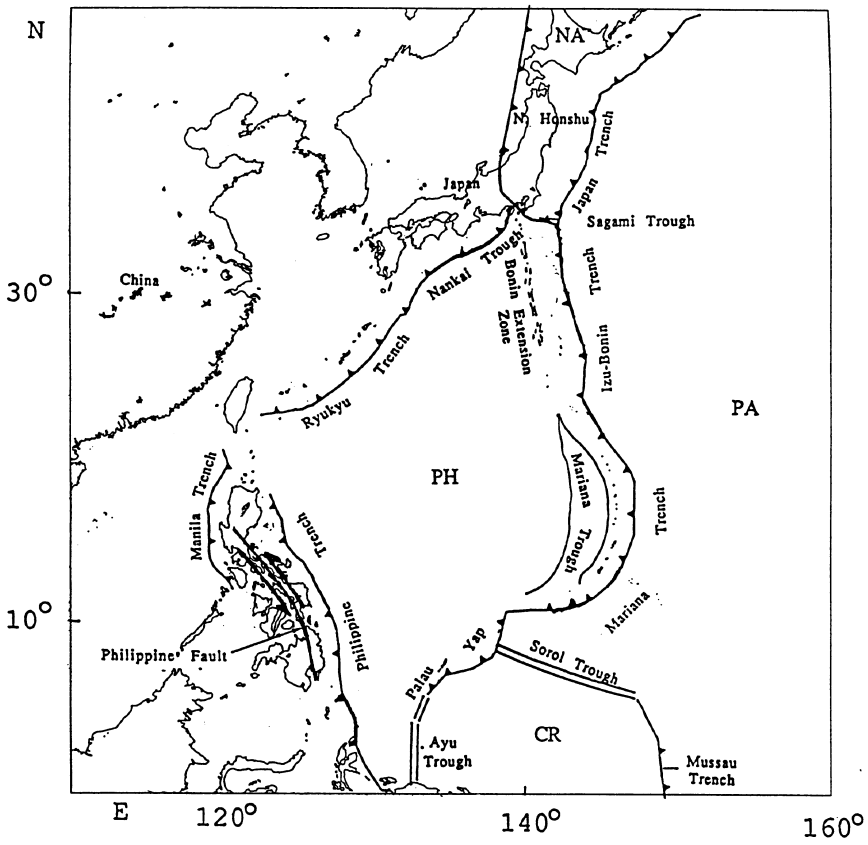


**Figure 1.** A simplified tectonic map of the Philippine Sea plate (adapted from Seno *et al.* 1993). (PH = Philippine Sea plate, PA = Pacific plate, CR = Caroline plate, NA = North American plate).

short-period waveform data recorded by the seismic station at Matsushiro, Japan (MAJO), Erdogan & Nowack (1993) constructed a composite seismic profile along the Japan subduction zone. In their regional *P*-wave velocity model, there is no evidence for anomalously fast *Vp* in the transition zone of the mantle near Japan. A similar conclusion for the Sea of Japan was reached by Tajima & Grand (1995) using sparse broadband waveform data.

To further investigate large-scale, lateral variations of *Vp* in the upper mantle beneath the Philippine Sea, we constrain the *P*-wave velocity structure in the upper mantle along the southwestern edge of the Philippine Sea Plate in this study. It is interesting to note that even though not nearly as prominent as the northern Philippine Sea anomaly, both tomographic studies of Fukao *et al.* (1992) and van der Hilst *et al.* (1993) reported somewhat faster regions of *Vp* in the middle of the transition zone (between depths of 480 and 570 km) beneath the southern Philippines. The tectonic origin of this anomaly, if it exists, is not clear because it does not appear to be connected with the anomaly beneath the northern Philippines Sea (Brudzinski *et al.* 1997).

In this investigation, we use *P* waves from shallow earthquakes recorded by a dense seismic array in Taiwan to construct a regional seismic profile along the Philippines. We will show that while the uppermost 300 km of the mantle is slower in *Vp* when compared with average earth models, only the uppermost portion of the transition zone just below the 410 km discontinuity has faster *Vp* velocities.

## DATA AND ANALYSIS

We used short-period seismograms recorded by a dense array of approximately 75 stations distributed over Taiwan and adjacent islands (Fig. 2). The array is jointly operated by the Taiwan Central Weather Bureau (CWB) and the Institute of Earth Sciences, Academia Sinica of Taiwan (Taiwan Telemetered Seismic Network, TTSN) (Wang 1989). Digital data have been available since 1987 and we used eight years of data collected by the array between 1987 and 1994 for the current analysis.

We selected shallow-focus earthquakes south of Taiwan to investigate the regional upper-mantle structure beneath the Philippines (Table 1). The earthquake locations are taken from monthly PDE locations of the US Geological Survey. Most of the 39 earthquakes used in this study are associated with westward subduction along the Philippine trench (Fig. 3). Near the island of Luzon, the South China Sea subducts eastward along the Manila trench beneath the Philippine Sea (Fig. 1) (e.g. Hamburger, Cardwell & Isacks 1983; Seno *et al.* 1993).

The midpoints between the centre of the Taiwan seismic array and the epicentres of earthquakes are the approximate positions of the bottoming points of the observed *P* waves. At these locations, the *P* waves propagate subhorizontally and are most sensitive to velocity structure near the bottoming depths. The seismic energy bottoms at transition-zone depths in the northern part of the Philippines and to the south (Fig. 3).

In the following analysis, we apply several techniques to

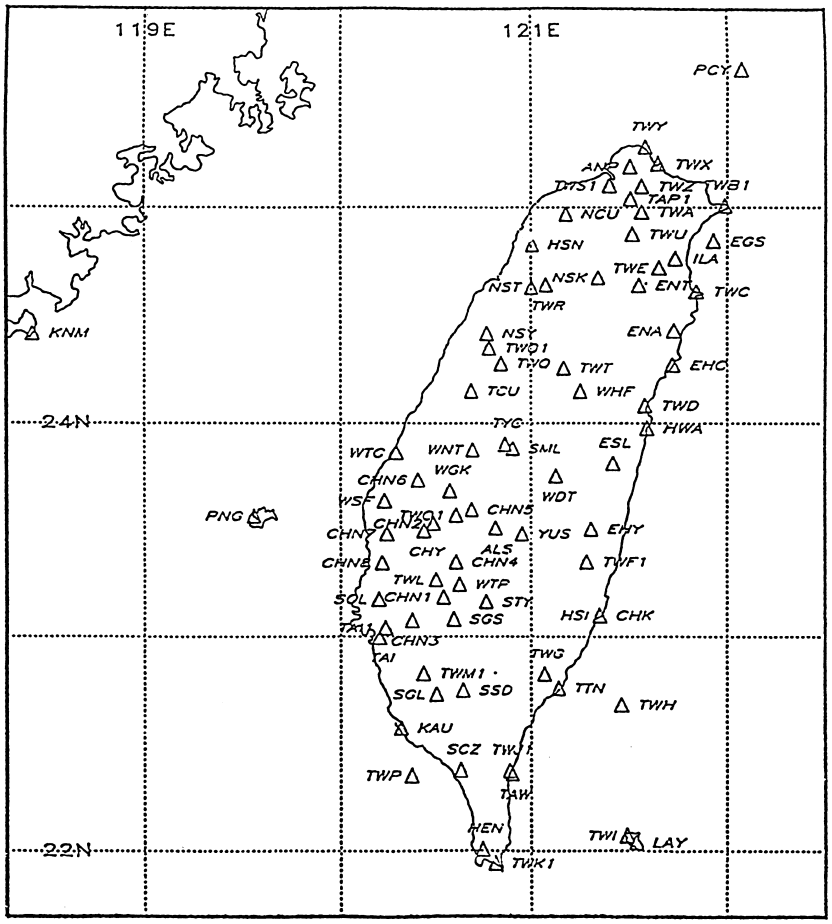


**Figure 2.** Map showing locations of three-component, digital, short-period seismic stations of the CWB/TTSN array in Taiwan.

analyse the data. First, we determine the traveltimes of first arrivals. Inversion of these traveltimes yields a smoothly varying velocity model. Second, we model waveforms of triplicate arrivals on individual event gathers to investigate seismic discontinuities in the upper mantle. Finally, we apply slant-stack analysis and downward continuation of waveforms to the entire seismic profile to obtain an average, regional velocity model.

## Traveltimes from first arrivals

We picked the timing of *P*-wave first arrivals interactively on a computer. After eliminating data of poor quality, the traveltimes were normalized to zero focal depth using the global reference model IASP91 (Kennett & Engdahl 1991) (Fig. 4a). Two limiting traveltime curves that contain approximately 80–90 per cent of the traveltime data, as well as an average curve between the upper and lower bounds, are also shown in Fig. 4(a).

In Fig. 4(b), the average traveltimes for the first arrivals are compared with the predicted first-arrival times of model IASP91. For distances less than 2000 km, the observed traveltimes are later than those predicted by model IASP91, suggesting that *Vp* in the uppermost mantle beneath the Philippines is slower than that of model IASP91. For distances greater than 2200 km, however, observed and predicted times are comparable. Thus, in comparison with the IASP91 model, a region of fast *Vp* must exist in the deeper part of the upper mantle that speeds up the traveltimes of deep-penetrating rays for distances greater than 2200 km.

To invert for velocity models, the three traveltime curves shown in Fig. 4(a) were first interpolated using splines and then converted to the $\tau$–$p$ domain, where $\tau$ is the intercept time and $p$ is the slope of the traveltime curve at a given distance. Inversions were then performed using the method of Diebold & Stoffa (1981), yielding *Vp* as a function of depth (Fig. 5). Because only first arrivals can be used in this procedure, these inversions produce smoothly varying models of *Vp*. For comparison, predicted first-arrival times from the IASP91 model have been inverted using the same method to obtain a smoothly varying version of the IASP91 model (dashed curve in Fig. 5).

Between depths of 50 and 300 km, all results of the inversion show slower velocities than the smoothly varying version of the IASP91 model. On the other hand, between depths of approximately 400 km and 550 km, models based on observed first arrivals are slightly faster in *Vp* than the IASP91 model. This conclusion based on the inversion of first arrivals is in agreement with the qualitative analysis based on Fig. 4(b).

## Modelling of waveforms

To equalize the pulse-shapes of signals from different earthquakes and to enhance the separation between first and

**Table 1.** Locations of 39 shallow earthquakes used in this study.

| EQ Number | EQ Label | Date | UTM Time (h:m:s) | Latitude (deg.) | Longitude (deg.) | Depth (km) | Magnitude ($m_b$) | Distance[A] (km) | Azimuth[A] (deg.) |
|---|---|---|---|---|---|---|---|---|---|
| 1 | C02 | Jan.08, 1993 | 19:26:38.8 | 18.14N | 121.02E | 25 | 5.4 | 648 | 180 |
| 2 | C03 | Jan.15, 1994 | 07:42:24.5 | 1.98N | 126.85E | 28 | 5.6 | 2512 | 165 |
| 3 | C11 | Mar.30, 1994 | 13:29:11.3 | 9.00N | 126.25E | 40 | 5.9 | 1749 | 161 |
| 4 | C13[R] | Apr.13, 1993 | 20:07:16.6 | 1.20N | 126.52E | 45 | 5.5 | 2588 | 166 |
| 5 | C15 | Apr.19, 1993 | 21:01:48.9 | 4.02N | 128.20E | 24 | 6.1 | 2339 | 160 |
| 6 | C18 | Apr.27, 1994 | 14:11:45.1 | 13.07N | 119.55E | 10 | 5.8 | 1217 | 187 |
| 7 | C19[R] | May 10, 1994 | 04:06:08.6 | 21.00N | 120.32E | 32 | 5.5 | 339 | 192 |
| 8 | C20 | May 13, 1994 | 20:12:27.8 | 7.97N | 123.19E | 33 | 5.6 | 1786 | 172 |
| 9 | C24 | May 30, 1993 | 22:34:03.8 | 0.62S | 124.21E | 75 | 5.6 | 2741 | 172 |
| 10 | C27 | June 04, 1993 | 10:49:33.6 | 3.73N | 128.50E | 20 | 5.9 | 2379 | 159 |
| 11 | C29[R] | June 06, 1992 | 23:29:32.3 | 3.67N | 126.95E | 44 | 5.5 | 2335 | 163 |
| 12 | C30 | June 09, 1992 | 00:31:56.3 | 8.47S | 111.10E | 64 | 5.9 | 3744 | 198 |
| 13 | C31[R] | June 09, 1994 | 16:22:22.0 | 13.26N | 124.28E | 76 | 5.8 | 1236 | 163 |
| 14 | C34[R] | July 04, 1991 | 11:43.10.4 | 8.10S | 124.68E | 29 | 6.2 | 3567 | 173 |
| 15 | C35[R] | July 05, 1994 | 10:09:22.6 | 10.43N | 125.32E | 29 | 5.5 | 1568 | 162 |
| 16 | C38[R] | July 24, 1994 | 21:57:27.4 | 10.65S | 113.27E | 34 | 6.0 | 3918 | 193 |
| 17 | C39[R] | Aug.02, 1992 | 05:50:11.6 | 0.88S | 127.58E | 19 | 5.8 | 2839 | 165 |
| 18 | C40 | Aug.09, 1992 | 19:49:44.1 | 4.01N | 126.36E | 73 | 6.1 | 2282 | 165 |
| 19 | C41[R] | Aug.19, 1993 | 06:48:26.9 | 13.32N | 124.16E | 71 | 5.3 | 1226 | 164 |
| 20 | C44 | Sept.11, 1992 | 22:24:52.2 | 4.15N | 126.46E | 46 | 5.4 | 2269 | 164 |
| 21 | C47 | Oct.13, 1991 | 00:57:53.2 | 2.45N | 127.73E | 27 | 5.6 | 2488 | 162 |
| 22 | C50 | Oct.13, 1994 | 05:04:24.9 | 1.21S | 127.91E | 11 | 6.1 | 2883 | 164 |
| 23 | C52 | Oct.18, 1991 | 19:10:10.4 | 7.82N | 122.13E | 36 | 5.3 | 1792 | 176 |
| 24 | C59[R] | Nov.13, 1991 | 11:12:13.2 | 8.36N | 126.37E | 36 | 6.1 | 1820 | 161 |
| 25 | C60[R] | Nov.21, 1991 | 12:38:28.5 | 5.78N | 126.83E | 73 | 6.0 | 2107 | 162 |
| 26 | C61 | Nov.22, 1993 | 03:00:55.8 | 5.89N | 126.23E | 38 | 5.7 | 2078 | 164 |
| 27 | C69[R] | Dec.23, 1991 | 19:57:35.7 | 3.43S | 127.31E | 33 | 5.2 | 3096 | 166 |
| 28 | T02[R] | Feb.08, 1990 | 07:15:32.2 | 9.76N | 124.69E | 26 | 6.2 | 1622 | 165 |
| 29 | T07[R] | June 14, 1990 | 07:40:56.2 | 11.76N | 121.89E | 18 | 6.0 | 1356 | 176 |
| 30 | T08[R] | Oct.03, 1987 | 10:16:26.27 | 5.45S | 131.01E | 73 | 6.4 | 3428 | 160 |
| 31 | T09 | May 30,1988 | 21:11:11:31 | 7.50S | 128.33E | 86 | 6.5 | 3569 | 166 |
| 32 | T10 | Oct.14, 1987 | 17:05:11:53 | 16.85N | 120.01E | 60 | 5.2 | 797 | 188 |
| 33 | T12 | July 16, 1991 | 09:39:21.7 | 16.52N | 120.93E | 16 | 5.6 | 827 | 181 |
| 34 | T13[R] | July 19, 1990 | 15:44:21.4 | 17.32N | 121.04E | 31 | 5.1 | 738 | 180 |
| 35 | T18 | Dec.23, 1987 | 10:10:20:55 | 0.16S | 124.88E | 60 | 5.7 | 2666 | 170 |
| 36 | T19 | June 09, 1992 | 00:31:56.3 | 8.47S | 111.10E | 64 | 5.9 | 3744 | 198 |
| 37 | T20 | Oct.28, 1988 | 10:37:52:75 | 0.35S | 122.19E | 15 | 5.7 | 2692 | 177 |
| 38 | T22 | Oct.25, 1990 | 11:01:38.7 | 8.31N | 126.46E | 44 | 5.9 | 1829 | 161 |
| 39 | T25 | Dec.23, 1990 | 21:03:03.7 | 0.66S | 127.39E | 32 | 5.6 | 2669 | 164 |

[R] Events used for record section.
[A] Distance and azimuth with respect to 24°N and 121°E

secondary arrivals, we performed a deterministic deconvolution on all waveforms. The deconvolution process also approximately removes the broadening of pulses caused by attenuation. An example of this type of deconvolution process is given by Erdogan & Nowack (1993). The deconvolved waveforms are then band-pass filtered from 0.1 to 1.2 Hz. For arrivals that have the same phase as the first arrivals, this process results in acausal wavelets centred at the arrival times. In addition to facilitating the combination of data from different events to form a composite seismic record section, deconvolution also results in better resolution in the slant-stacking of the waveform data, an intermediate step necessary for wavefield analysis.

The last step in data processing is the removal of station residuals to account for variations in near-surface structures. We used the average arrival times in Fig. 4(b) as the basis for the station corrections. Such corrections remove fluctuations of first-arrival times from the baseline and thus on average minimize random errors from local structure beneath each station and hypocentre mislocations. These effects are further reduced when the relative timing between triplicate, secondary arrivals and first arrivals is considered in the waveform analysis.

To constrain the nature of seismic discontinuities, we modelled observed short-period body waves, including triplicate arrivals, by computing synthetic seismograms using the WKBJ method (Chapman 1978; Chapman *et al.* 1988). Combining the results of waveform modelling for individual event gathers and those from slant-stack analysis of the entire seismic profile, we derived a preferred velocity model TS.406 that includes two upper-mantle discontinuities at depths of 406 and 662 km (Fig. 6 and Table 2).

Fig. 7 shows examples of waveform modelling at increasing distance ranges, illustrating the major features of model TS.406. Fig. 7(a) compares observed and synthetic seismograms for event C59 at distances between 1660 and 1770 km. Important features of the observed waveforms, including both the first arrivals and the later arrivals in the next few seconds, have been approximately matched by synthetic seismograms. The wide-angle branch from the low-velocity zone (A), the forward and wide-angle branches above 406 km (B) and the refracted branch in the transition zone (C) are well separated on the observed waveform at a distance of 1660 km. The timing of the wide-angle reflection from the '410 km' discontinuity constrains the average *Vp* above the discontinuity, while the distance over which this arrival is observed on different seismic gathers determines the size of the jump in *Vp* across the discontinuity. From this gather, the near end of the triplication

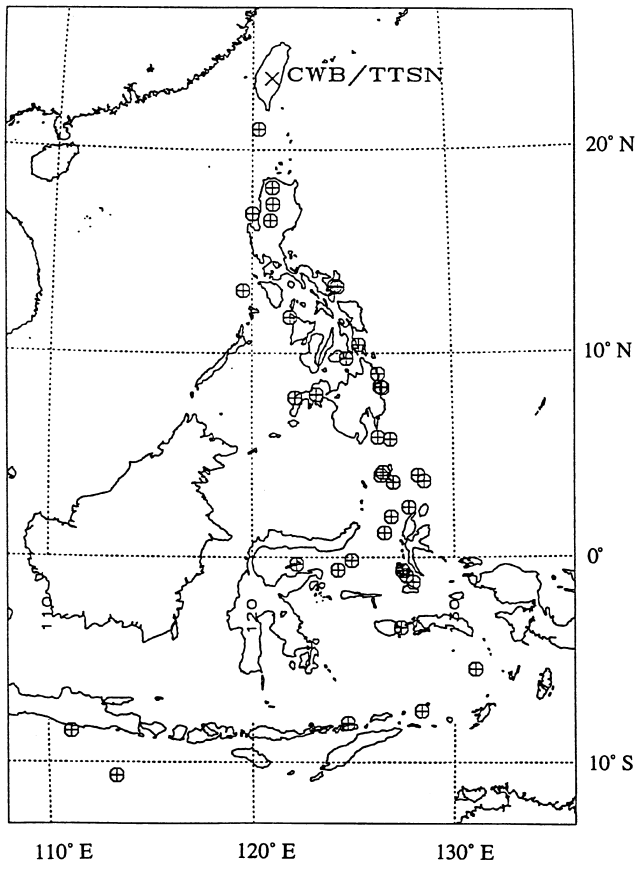


**Figure 3.** Map showing epicentres of shallow earthquakes (targets) south of Taiwan used in this study.

due to the '410 km' discontinuity extends to distances less than 1660 km.

Fig. 7(b) shows a seismic section from event C60, with the letter D marking the wide-angle and forward branches of the predicted traveltimes due to the discontinuity at 662 km. At distances between 2050 and 2250 km, cusps in the traveltime curve (B and D in Fig. 7b) due to both the '410' and the '660 km' discontinuities are observed at reduced traveltimes of about 55 s and 57 s, respectively. The far end of the cusp due to the '410 km' discontinuity can be traced out to a distance near 2250 km. Combined with results from Fig. 7(a), triplicated arrivals from the '410 km' discontinuity are observed over a distance range of more than 600 km. This observation indicates a contrast in *Vp* of approximately 5.5 per cent across this discontinuity.

The near end of the cusp due to the '660 km' discontinuity initiates near a distance of 2050 km (Fig. 7b). Meanwhile, the far end of this cusp can be traced out to a distance of approximately 3150 km (Fig. 8). This observation leads to approximately a 5.4 per cent jump in *Vp* over the '660 km' discontinuity in model TS.406. In addition, clear moveout of the arrival times over a distance range of several hundred kilometres for all three triplicate arrivals constrains the *Vp* near this discontinuity (Fig. 7c).

On the basis of modelling of waveforms and traveltimes of triplicated arrivals in a number of examples similar to those shown in Fig. 7, the uncertainties in the depths of discontinuities are of the order of $\pm 5$ km. Additional uncertainties in the depths of the discontinuities result from application of the static corrections. In order to estimate this contribution to the depth errors, the smooth velocity models shown in Fig. 5 for the lower- and upper-bound curves in Fig. 4(a) were used to compute two-way traveltimes. From the difference in these times, an additional error in the discontinuity depths from the static corrections is estimated to be of the order of $\pm 5$ km, resulting in a total error in the upper-mantle discontinuity depths of $\pm 10$ km.

### Wavefield analysis

Assuming lateral homogeneity along the profile, wavefield data consisting of spatially unaliased waveforms can be analysed to image the velocity structure at depth. Two linear transformations of the wavefield data are involved in this analysis: slant-stack and downward continuation. The first transformation (slant-stack) takes the wavefield data from the $T$–$X$ (traveltime and distance) domain to the $\tau$–$p$ domain. Using an initial velocity model $V(z)$ with depth, the $\tau$–$p$ wavefield data can then be downward continued to the $p$–$z$ domain (Clayton & McMechan 1981). The downward continuation is an iterative procedure, and convergence is achieved when the maxima on the downward-continued wavefield coincide with the velocity model. The velocity model is then transformed to an equivalent, spherical earth model (Aki & Richards 1980).

We constructed a seismic profile by combining the event gathers (Table 1). Following deconvolution and station corrections as described in earlier sections, we tapered and muted the waveform data outside of a time window from 5 s before and 22 s after the first arrivals to exclude noisy coda waves. After eliminating overlapping traces and seismograms of low signal-to-noise ratios, 159 seismograms from distances between 150 and 4000 km were used for slant stacking. For clarity, Fig. 8 shows the resulting seismic profile for a reduced distance range of 900 km to 3400 km.

For slant stacking, we mapped the seismic record section into the $\tau$–$p$ domain by using a range for the inverse of the ray parameter from 7 to 14 km s$^{-1}$ at 0.01 km s$^{-1}$ intervals, and $\tau$ values ranging from 0.0 to 140.0 s at increments of 0.05 s. The wavefield in the $\tau$–$p$ domain was then downward continued with a suite of possible velocity models to obtain the corresponding wavefields in the $V$–$z$ domain. The resulting wavefield in the $V$–$z$ domain for model TS.406 after earth flattening is shown in Fig. 9. In general, model TS.406 corresponds to the largest amplitudes in the $V$–$z$ wavefield data, although there are some minor deviations, details of which are individually controlled by waveform modelling of the individual event gathers. On the basis of the width of the largest pulses in the downward-continued wavefield (Fig. 9), uncertainties in *Vp* from the slant-stack analysis are of the order of $\pm 0.15$ km s$^{-1}$. Additional uncertainties resulting from the static corrections can be estimated from the range of smoothly varying velocity models in Fig. 5 derived from the upper- and lower-bound curves in Fig. 4(a). For depths below 300 km, the overall uncertainty in *Vp* is approximately $\pm 0.2$ km s$^{-1}$.

## DISCUSSION

Fig. 6 compares model TS.406 for the southwestern edge of the Philippine Sea plate with selected global and regional models for the upper mantle. Using a single station in central

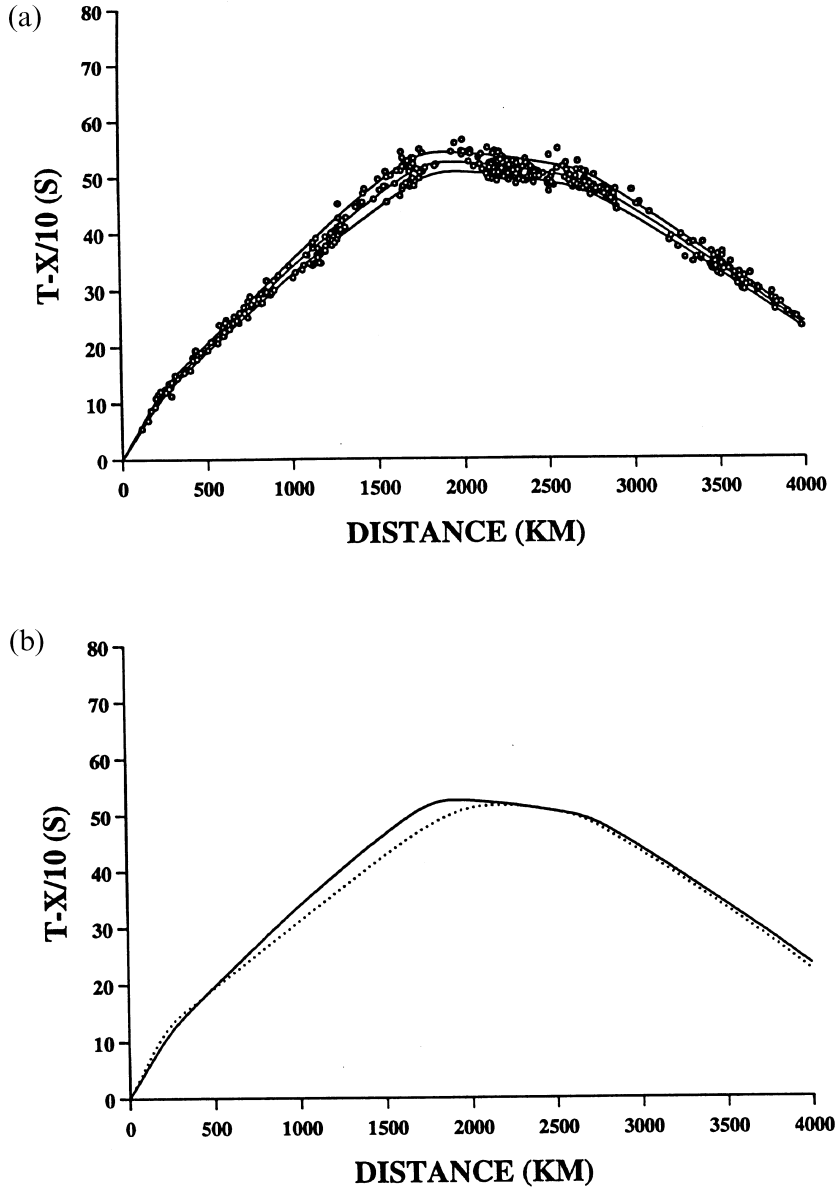


**Figure 4.** (a) Traveltimes of first arrivals (circles) for events located south of Taiwan. The lower and upper solid curves bound approximately 80–90 per cent of the data. The middle curve is the average of the two limiting curves. (b) Comparison of observed, average first-arrival times (solid line) and predictions based on the IASP91 model (dotted line).

Japan, Erdogan & Nowack (1993) performed an analysis similar to the present study to derive an average upper-mantle model ('model N50').

Most of the data used by Erdogan & Nowack (1993) sample a region along the Japan arc, with sparse coverage of the northwestern edge of the Philippine Sea. Model N50 has a low-velocity zone (LVZ) in the uppermost mantle, below which the gradient of *Vp* in the transition zone is similar to that of the global model IASP91. Model TS.406, on the other hand, is based on array data recorded in Taiwan, sampling the southwestern edge of the Philippine Sea plate (Fig. 1). When compared with model N50, as well as models IASP91 (Kennett & Engdahl 1991) and PREM (Dziewonski & Anderson 1982), the latter two being commonly used average earth models, model TS.406 allows for a small LVZ but generally its *P*-wave velocity is still slower than these other models above a depth of 300 km (Fig. 6). For example, at depths above 300 km, model TS.406 is slower than IASP91 by 1.5 per cent. The *P*-wave velocity then speeds up in the top portion of the transition zone, leading to a jump of 5.5 per cent at the '410 km' discontinuity and a correspondingly lower gradient in *Vp* over the thickness of the transition zone compared to other models. These features of model TS.406 are also constrained by travel-times of the first arrivals (Figs 4 and 5).

Kennett (1993) compiled the results from a number of earlier models for the upper mantle and found a range of 2.5 to 5.8 per cent in the contrast of *Vp* across the '410 km' discontinuity. A velocity contrast of 5.5 per cent at a depth of 406 km found in this study is below the upper bound of the range from other studies. The corresponding lower gradient of 0.0027 km $s^{-1}$ $km^{-1}$ in *Vp* is above the lower bound of the range (0.002 to 0.005 km $s^{-1}$ $km^{-1}$) reported by Kennett

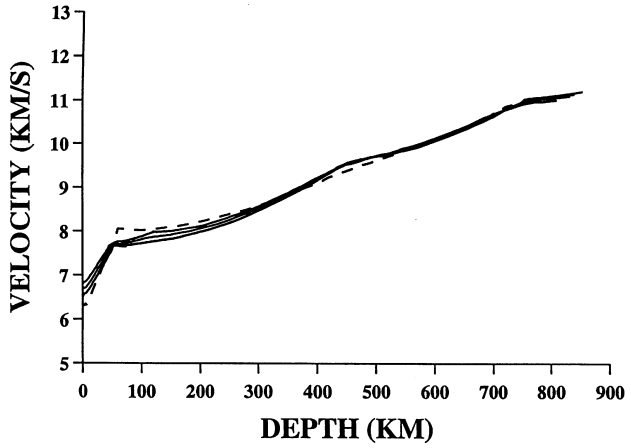


**Figure 5.** Result of inversion (solid curves) using the three traveltime curves shown in Fig. 4(a). The dashed curve is the result derived from first-arrival times predicted by the IASP91 model.

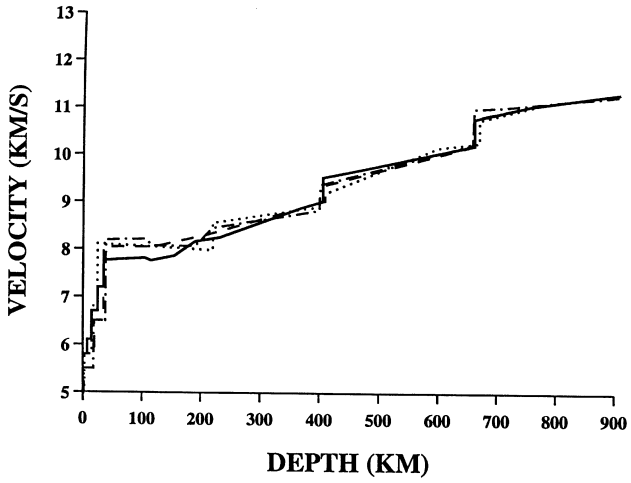


**Figure 6.** A comparison of model TS.406 from this study (solid curve) with models IASP91 (dashed curve), PREM (dotted curve) and model N50 from Erdogan & Nowack (1993) (dash–dot curve).

(1993). As such, a faster *P*-wave velocity beneath the Philippines appears to occur only in the top portion of the transition zone, at depths considerably shallower than the range of 480–570 km based on tomographic studies of first arrivals (Fukao *et al.* 1992; van der Hilst *et al.* 1993).

When averaged over the depths of 406 and 571 km, the *P*-wave velocity in model TS.406 is 1.2 per cent higher than the IASP91 model. In contrast, the Northern Philippine Sea Anomaly has an increase in velocity of 2 per cent in the bottom half of the transition zone (Brudzinski *et al.* 1997). Along our profile, we found no evidence for anomalous *Vp* at depths below 550 km, as a jump in velocity of 5.4 per cent at 662 km falls in the middle of the range expected for the '660 km' discontinuity (3.6 to 7.3 per cent, Kennett 1993). This is in contrast with the recent global estimate of a smaller jump in *Vp* of only 2 per cent found by Estabrook & Kind (1996) using precursors to the *PP* phase.

Other recent studies have also investigated variations in the depths to major discontinuities in the upper mantle. Such variations are important for understanding the relationship

**Table 2.** *P*-wave velocites for model TS.406.

| Depth (km) | Velocity (km/s) |
|---|---|
| 0.0 | 5.80 |
| 7.5 | 5.80 |
| 7.6 | 6.10 |
| 15.0 | 6.10 |
| 15.1 | 6.70 |
| 25.0 | 6.70 |
| 25.1 | 7.20 |
| 35.0 | 7.20 |
| 35.1 | 7.76 |
| 71.0 | 7.79 |
| 105.0 | 7.82 |
| 115.0 | 7.76 |
| 155.0 | 7.86 |
| 190.0 | 8.16 |
| 190.1 | 8.16 |
| 231.0 | 8.25 |
| 371.0 | 8.89 |
| 406.0 | 9.02 |
| 406.1 | 9.52 |
| 471.0 | 9.69 |
| 571.0 | 9.96 |
| 662.0 | 10.21 |
| 662.1 | 10.77 |
| 671.0 | 10.80 |
| 760.0 | 11.06 |
| 771.0 | 11.08 |
| 871.0 | 11.25 |
| 971.0 | 11.42 |
| 1000.0 | 11.46 |

between the positions of phase/chemical boundaries and perturbations in mineralogical composition and temperature (e.g. Anderson & Bass 1986; Anderson 1989). Using the long-period signal (~20 s) of *SS* precursors converted off major discontinuities of the upper mantle, Flanagan & Shearer (1998) found depths of 418 and 664 km for the '410 km' and '660 km' discontinuities beneath the Philippines. Shearer (1991, 1996) also inferred the existence of a discontinuity near 520 km. We did not find enough evidence in our data to support the existence of a 520 km discontinuity along our profile.

Flanagan & Shearer (1998) inferred a somewhat greater depth of the '410 km' discontinuity for the region south of Taiwan than that of model TS.406. In estimating the apparent depths, they assumed *S*-wave velocities from the PREM model (Dziewonski & Anderson 1981) and attempted to correct the PREM model for crustal thickness and for *S*-velocity heterogeneities. However, for depths above 300 km, *Vp* of model TS.406 is slower than that of PREM (Fig. 7). If a similar difference exists in the *S*-wave velocities, then the true depth to the '410 km' discontinuity should be shallower than 410 km in order to maintain a given observed vertical traveltime interval.

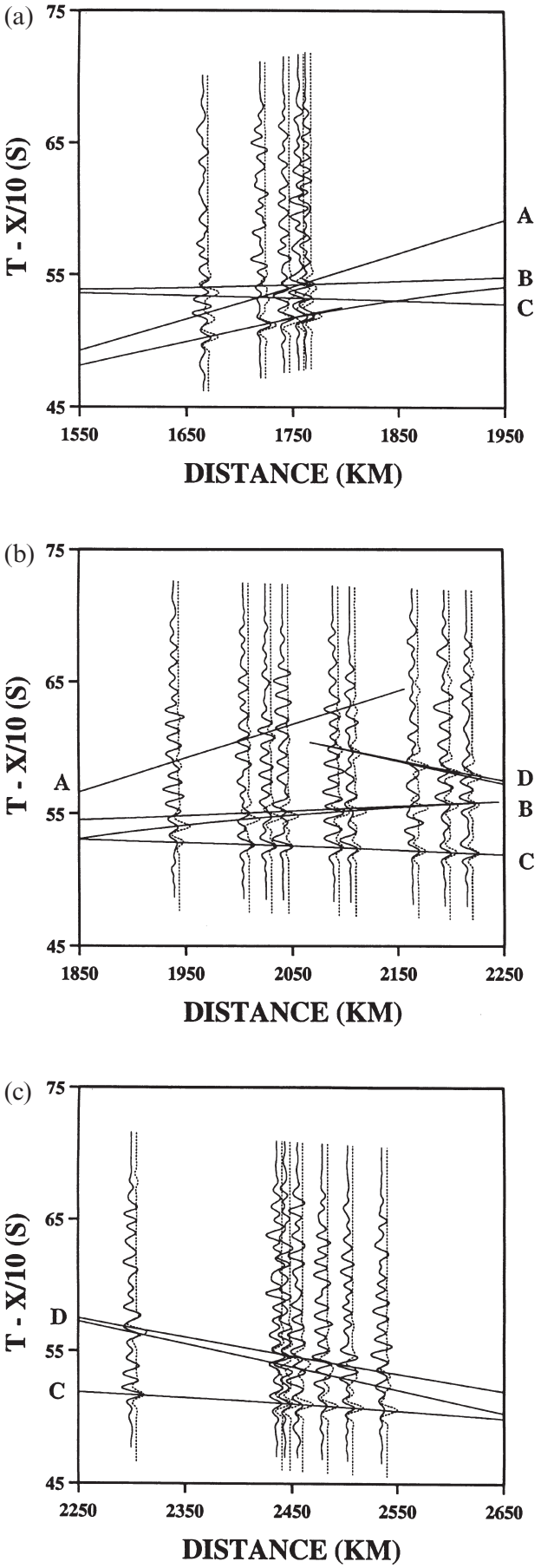


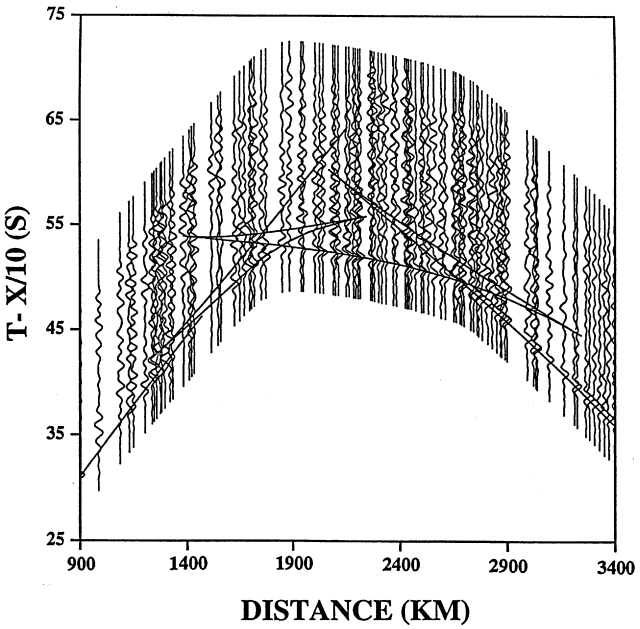


**Figure 8.** Deconvolved seismograms between distances of 900 and 3400 km. The traveltime curves are based on model TS.406 (Fig. 6).

In any case, both velocity and depth are estimated in a self-consistent manner in model TS.406. It provides a regional *P*-wave velocity model that can serve as a basis for the investigation of fine-scale structures in the upper mantle and the lithosphere beneath the southwestern edge of the Philippine Sea plate.

## CONCLUSIONS

Using both traveltimes and waveform data from numerous earthquakes under the Philippines and a dense array of short-period seismic stations in Taiwan, we have investigated the *P*-wave velocity structure of the upper mantle beneath the southwestern edge of the Philippine Sea plate. When compared to average earth models, the traveltimes of first arrivals alone indicate that for this region, *Vp* of the upper mantle above the transition zone is slow. Below this depth, however, *Vp* is faster than usual, such that no significant traveltime anomaly is present at distances greater than approximately 2500 km. Modelling of triplicate waveforms from the '410 km' and '660 km' discontinuities and the results from downward continuation of the observed *P* wavefield show that *Vp* in the

**Figure 7.** A comparison of deconvolved seismograms for event C59 (solid traces) with synthetic seismograms (dotted traces) and traveltimes (solid curves) predicted by model TS.406. For the traveltime curves, the letter A shows the branch associated with wide-angle reflections from the bottom of the low-velocity zone, B shows the forward and wide-angle branches above the discontinuity at a depth of 406 km and C shows the forward, refracted branch inside the transition zone. (b) A comparison of deconvolved seismograms for event C60 with synthetic seismograms and traveltimes predicted by model TS.406. The symbols are the same as in (a). In addition, the letter D shows the wide-angle and forward branches above the discontinuity at a depth of 662 km. (c) A comparison of deconvolved seismograms for event C03 with synthetic seismograms and traveltimes predicted by model TS.406. The symbols are the same as in (b).

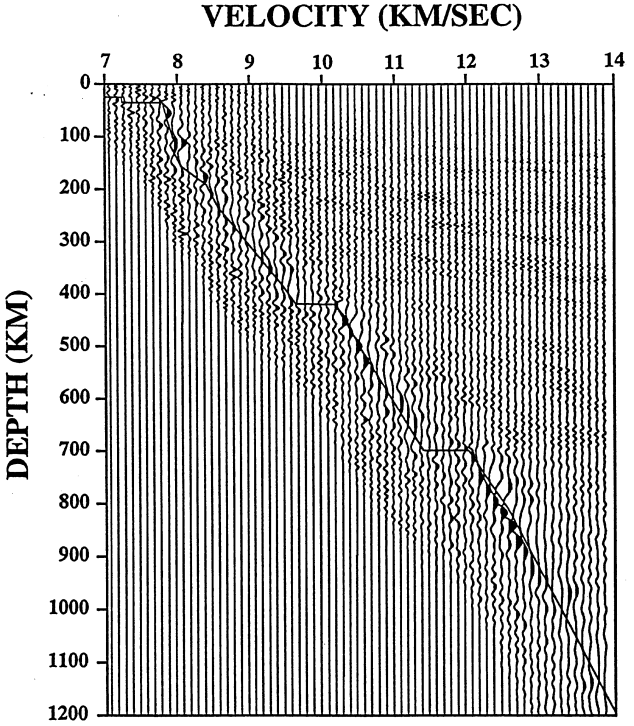


**Figure 9.** Slant-stacked and downward-continued wavefield of the seismic profile. The solid line is the earth-flattened version of model TS.406.

upper portion of the transition zone, between depths of 406 and 571 km, is approximately 1.2 per cent faster than that of the IASP91 model. The top of the transition zone is marked by a contrast in *Vp* of 5.5 per cent at a depth of 406 km. In our preferred model, the transition zone is characterized by a moderate, linear gradient of 0.0027 km $s^{-1}$ $km^{-1}$ down to its base at a depth of 662 km. The data do not require the presence of a 520 km discontinuity. Also, in contrast to previous results from tomographic studies that do not include secondary arrivals and wavefield data, there is no evidence for anomalously fast *Vp* in the middle of the transition zone. Near the bottom of the transition zone, the lack of anomalous *P*-wave velocities along the southwestern edge of the Philippine Sea is in marked contrast to the fast *Vp* (by $\sim$2 per cent) associated with the Northern Philippine Sea anomaly.

## ACKNOWLEDGMENTS

We would like to thank Y. H. Yeh and T. Shin for permitting us access to CWB-TTSN data. P. Shearer and an anonymous reviewer offered helpful suggestions. This research was supported by NSF grants EAR94-0408 and EAR93-16012 (W-PC) and grant EAR94-05167 (RLN).

## REFERENCES

Aki, K. & Richards, P.G., 1980. *Quantitative Seismology,* Freeman, San Francisco.

Anderson, D.L., 1989. *Theory of the Earth,* Blackwell Scientific, Boston, Mass.

Anderson, D.L. & Bass, J.D., 1986. Transition region of the Earth's upper mantle, *Nature,* **320,** 321–328.

Brudzinski, M.R., Chen, W.-P., Nowack, R.L. & Huang, B.S., 1997. Variations of *P*-wave speeds in the Mantle Transition Zone beneath the northern Philippine Sea Plate, *J. geophys. Res.,* **102,** 11 815–11 828.

Chapman, C.H., 1978. A new method for computing synthetic seismograms, *Geophys. J. R. astr. Soc.,* **54,** 481–518.

Chapman, C.H., Jen-Yi, C. & Lyness, D.G., 1988. The WKBJ seismogram algorithm, in *Seismological Algorithms: Computational Methods and Computer Programs,* pp. 47–74, ed. Doornbos, D.J., Academic Press, San Diego.

Clayton, R.W. & McMechan, G.A., 1981. Inversion of refraction data by wavefield continuation, *Geophysics,* **46,** 860–868.

Diebold, J.B. & Stoffa, P.L., 1981. The traveltime equation, tau–p mapping, and inversion of common midpoint data *Geophysics,* **46,** 238–234.

Dziewonski, A.M. & Anderson, D.L., 1981. Preliminary reference earth model, *Phys. Earth planet. Inter.,* **25,** 297–356.

Erdogan, N. & Nowack, R.L., 1993. Slant-stack velocity analysis for one-dimensional upper mantle structure using short short-period data from MAJO, *Pageoph,* **141,** 1–24.

Estabrook, C.H. & Kind, R. 1996. The nature of the 660-kilometer upper-mantle seismic discontinuity from precursors to the *PP* phase, *Science,* **274,** 1179–1182.

Flanagan, M.P. & Shearer, P.M., 1998. Global mapping of topography on transition zone velocity discontinuities by stacking *SS* precursors, *J. Geophys. Res.,* **103,** 2673–2692.

Fukao, Y., Obatashi, M., Inoue, H. & Nenbai, M., 1992. Subducting slabs stagnant in the mantle transition zone, *J. geophys. Res.,* **97,** 4809–4822.

Hamburger, M.W., Cardwell, R.K. & Isacks, B.L., 1983. Seismotectonics of northern Philippine Island Arc, in *The Tectonic and Geologic Evolution of Southeast Asian Seas and Islands: Part 2,* ed. Hayes, D.E, *Geophys. Monogr.,* **27,** 1–22.

Kennett, B.L.N., 1993. Seismic structure and heterogeneity in the upper mantle, in *Relating Geophysical Structures and Processes: The Jeffreys Volume,* eds Aki, K. & Dmowska, R., *Geophys. Monogr.,* **76,** 53–66.

Kennett, B.L.N. & Engdahl, E.R., 1991. Traveltimes for global earthquake location and phase identification, *Geophys. J. Int.,* **105,** 429–465.

Seno, T., Stein, S. & Gripp, A.E., 1993. A model for the motion of the Philippine sea plate consistent with NUVEL-1 and geological data, *J. geophys. Res.,* **98,** 17 941–17 948.

Shearer, P., 1991. Constraints on upper mantle discontinuities from observations of long period reflected and converted phases, *J. geophys. Res.,* **96,** 18 147–18 182.

Shearer, P., 1996. Transition zone velocity gradients and the 520-km discontinuity, *J. geophys. Res.,* **101,** 3053–3066.

Tajima, F. & Grand, S.P., 1995. Evidence of high velocity anomalies in the transition zone associated with southern Kurile subduction zone, *Geophys. Res. Lett.,* **22,** 3139–3142.

van der Hilst, R.D. & Seno, T., 1993. Effect of relative plate motion on the deep structure and penetration depth of slabs below the Izo-Bonin and Mariana Island arcs, *Earth planet. Sci. Lett.,* **120,** 395–407.

van der Hilst, R.D., Engdahl, E.R., Spakman, W. & Nolet, G., 1991. Tomographic imaging of subducted lithosphere below northwest Pacific island arcs, *Nature,* **353,** 37–43.

van der Hilst, R.D., Engdahl, E.R. & Spakman, W., 1993. Tomographic inversion of *P* and *pP* data for aspherical mantle structure below the northwest Pacific region, *Geophys. J. Int.,* **115,** 264–302.

Wang, J.H., 1989. The Taiwan telemetered seismographic network, *Phys. Earth planet. Inter.,* **58,** 9–18.